Silver-doped calcium silicate sol-gel glasses with a cotton-wool-like structure for wound healing

Ju, Qun; Zenji, Takuya; Maçon, Anthony LB; Norris, Elizabeth; Poologasundarampillai, Gowsihan; Obata, Akiko; Jones, Julian R; Kasuga, Toshihiro

DOI:
10.1016/j.msec.2021.112561

Document Version
Peer reviewed version

Silver-doped calcium silicate sol-gel glasses with a cotton-wool-like structure for wound healing

Qun Ju[1], Takuya Zenji[1], Anthony L.B. Maçon[1], Elizabeth Norris[2], Gowsihan Poologasundarampillai[3], Akiko Obata[1*], Julian R Jones[2], Toshihiro Kasuga[1]

[1] Graduate School of Engineering, Nagoya Institute of Technology, Gokiso-cho, Showa-ku, Nagoya, 466-8555, Japan
[2] Department of Materials, Imperial College London, South Kensington Campus, London, SW7 2AZ, UK
[3] School of Dentistry, Institute of Clinical Sciences, University of Birmingham, 5 Mil Pool Way, Edgbaston, Birmingham, B5 7EG, UK

Corresponding author
Akiko Obata
obata.akiko@nitech.ac.jp

Silver-doped calcium silicate sol-gel glasses with a cotton-wool-like structure for wound healing

Abstract

Skin has excellent capacity to regenerate, however, in the event of a large injury or burn skin grafts are required to aid wound healing. The regenerative capacity further declines with increasing age and can be further exacerbated with bacterial infection leading to a chronic wound. Engineered skin substitutes can be used to provide a temporary template for the damaged tissue, to prevent/combat bacterial infection and promote healing. In this study, the sol-gel process and electrospinning were combined to fabricate 3D cotton-wool-like sol-gel bioactive glass fibers that mimic the fibrous architecture of skin extracellular matrix (ECM) and deliver metal ions for antibacterial (silver) and therapeutic (calcium and silica species) actions for successful healing of wounds. This study investigated the effects of synthesis and process parameters, in particular sintering temperature on the fiber morphology, the incorporation and distribution of silver and the degradation rate of fibers. Silver nitrate was found to decompose into silver nanoparticles within the glass fibers upon calcination. Furthermore, with increasing calcination temperature the nanoparticles increased in size from 3 nm at 600°C to ~25 nm at 800°C. The antibacterial ability of the Ag-doped glass fibers decreased as a function of the glass calcination temperature. The degradation products from the Ag-doped 3D non-woven sol-gel glass fibers were also found to promote fibroblast proliferation thus demonstrating their potential for use in skin regeneration.

Keywords

Bioactive glass, Electrospinning, Wound healing, Antibacterial property, Cotton-wool-like structure

1. Introduction

Skin provides a barrier against external aggression, whilst also sensing and regulating fluid homeostasis (sweating) [1]. Injury triggers the complex process of wound healing, which restores the lost structure and function. This process can be divided into four distinct phases: hemostasis, inflammation, proliferation, and remodeling. However, in adult skin healing, a once functional tissue repair can become a disorganized patch of cells (mainly fibroblasts) and ECM (mainly collagen) that is commonly referred to as a scar tissue, which lacks many of the functional attributes of skin [2].

Most wounds are colonized by bacteria to varying degrees, but when the body's defenses are weakened or a colonization agent is persistent, the level of colonization becomes critical, leading to chronic infection. Chronic wounds are defined as those that fail to proceed through the normal phases of wound healing in an orderly and timely manner [3, 4]. They are an ideal environment for biofilm formation. Increasing rates of obesity and diabetes within our ageing population also impairs wound healing [5]. Healing of chronic wounds are affected by many factors, such as local infection, comorbidity, wound pain, oxygen supply to the wound area, and patient adherence to treatment. Antibiotics delivered locally or systemically are the common mode of treatment to combat infection. However, antibiotics are not effective against biofilms and their prolonged use contributes to antimicrobial resistance. Better treatment options are required to combat chronic wounds. In addition to combatting infection, the treatment should promote tissue regeneration leading to scar-free healing. Novel synthetic bioactive materials are emerging as potential candidates for this major unmet need [6, 7].

Regenerative materials are those that actively recruit progenitor cells and provide appropriate cues to promote the regeneration of skin [8, 9]. These chemical cues can be classified into two depending of their nature: organic cues, such as growth factors [10, 11], or inorganic cues, such as metal ions and inorganic species [12]. Bioactive glasses (BGs) have great potential to be used as biomaterials for wound healing [6, 7]. Lin *et al.* combined sol-gel derived bioactive glass 58S ($60SiO_2$-$36CaO$-$4P_2O_5$ mol%) and melt-derived 45S5 ($46.1SiO_2$-$26.9CaO$-$24.4Na_2O$-$2.6P_2O_5$ mol%) bioactive glass powders with Vaseline and applied these as ointment on diabetic rat skin wounds [13]. Both BGs were found to accelerate the wound healing process, compared to a control group consisting of BG-free Vaseline[13]. They concluded that the ions released from BGs were able to stimulate the secretion of angiogenic growth factors from fibroblasts to achieve increased vascularization. This supported earlier *in vitro* work that showed Bioglass dissolution products promoted VEGF expression from fibroblasts [14-16], later *in vitro* work [17, 18] and *in vivo* work [19].

Conventional melt-derived glasses are made by the quenching of a melt, whereas sol-gel glasses are produced through the hydrolysis of alkoxide precursors than enable bottom-up assembly of the silicate glass network at room temperature [20], giving rise to nanoporous glasses with high surface area after drying and calcination. Recently, we developed bioactive sol-gel glass scaffolds with a 3D cotton-wool-like structure by electrospinning the sol [21]. The composition of the glasses was $(100\text{-}x)SiO_2 - xCaO$ (x = 0, 10, 20, 30, and 40 mol%), wherein the calcium content of the sol and the relative humidity of the electrospinning environment were found to influence the 3D cotton-wool-like morphology. Human dermal fibroblast (HDF) metabolic activity after being cultured in media conditioned with $70SiO_2$-$30CaO$ (70S30C) and 80S20C BGs was

similar to that of control sample (cell culture plastic). The capacity of HDFs to produce vascular endothelial growth factor (VEGF) was enhanced in comparison with control.

Here, we developed Ag-doped 70S30C glasses with 3D cotton-wool-like structure and investigated their antibacterial properties. Silver is of particular interest since it is a well-known and clinically used antibacterial agent. Silver has a broad spectrum of action, possessing strong biocidal effects on a variety of antibiotics resistant bacteria, such as Gram-negative bacteria, *Escherichia coli* (*E. coli*), Gram-positive bacteria, *Straphylococcus aureus* (*S. aureus*) [22] and methicillin-resistant *S. aureus* (MRSA) [23]. Following the antimicrobial studies on the first silver-containing sol-gel glass particles [24], various types of Ag-doped BGs have been developed [23-52]. Saha *et al*. successfully prepared Ag-doped borosilicate glasses fibers with cotton-wool-like structure via electrospinning and demonstrated antibacterial efficacy on *S. aureus* and the activation property for endothelial cell migration [53]. Qin *et al*. reported Ag-doped ordered mesoporous silicate glass fibers and demonstrated a dose-dependent behavior on antibacterial efficacy and cell compatibility [54], where 2 mg/mL of the glass gave both antibacterial efficacy and cell compatibility whilst 200 mg/mL provided only antibacterial efficacy. While the Ag is hypothesized to enter the glass network as a network modifier, Carta et al. reported evidence of Ag nanoparticle formation inside Ag-doped sol-gel derived microparticles through neutron diffraction[40]. To date, reports on Ag-doped sol-gel glass scaffolds do not provide insight on the speciation of the silver nor its size or distribution within the glass fibers. This is important as the size of Ag particles has been reported to play a strong role in the antibacterial activity of silver [55]. There is also very little information on how the presence of Ag nanoparticles in a bioactive glass, and their size, influences the glass degradation, silver ion release and thus antibacterial activity.

This study gives a thorough investigation of the effect of synthesis and process parameters on the resulting $70SiO_2$-$(30-x)CaO$-xAg_2O BGs fiber morphology, incorporation and distribution of silver and its release profile. Furthermore, antibacterial and cell compatibility were also assessed to form an understanding of structure-property-function of the glass fibers.

2. Materials and Methods

2.1. Preparation of sol-gel glasses with cotton-wool-like structure

A sol of ethanol (Wako Pure Chemical Industries, Ltd.), 1 N HNO_3 (Wako Pure Chemical Industries, Ltd.), and tetraethylorthosilicate (TEOS) (Sigma-Aldrich) with a TEOS:ethanol:water:HNO_3 molar ratio of 1:2:3:0.05 was prepared in a PTFE container and stirred vigorously. After stirring for 1 h, $Ca(NO_3)_2 \cdot 4H_2O$ (Wako Pure Chemical Industries, Ltd.) was added to sol of nominal composition 70 mol% SiO_2 and 30 mol% CaO. The 70S30C sol was poured in a closed container was then stirred for 24 h and subsequently aged at 40 °C oven for 17 h to increase the viscosity of the sol.

Antibacterial sol-gel glasses $70SiO_2$-$(30-x)CaO$-xAg_2O (x = 0, 1, 2) were produced by substituting Ag_2O for CaO using $AgNO_3$ (Wako Pure Chemical Industries, Ltd.) and introducing the salts of silver and calcium in the sol at the same time. Aluminum foil was used to cover the reaction vessel to prevent any oxidation of silver due to UV exposure. In a separate beaker, poly(vinylbutyral) (PVB) (Butvar® B-98, Sigma-Aldrich) was dissolved in ethanol at 10 wt% and mixed with the aged sol at an equivalent volume (5 mL), giving an solution with appropriate viscosity for electrospinning [56]. Table 1 lists the quantities of the reagents used in this work.

Humidity affects electrospinning of the sol greatly[21], so the solution was electrospun in a closed chamber in which the relative humidity during the

electrospinning process was set to around 33 %. The solution was loaded in a syringe pump (FP-W-100, Melquest) and spun into a rectangular container covered with aluminum foil placed at 150 mm of the electrospinning needle. A power supply connected to the metal syringe needle (22 gauge) was used to create a high potential between the needle and collector to allow electrospinning. The electrospinning conditions are 32-35 % of humidity, 10-13 kV of applied voltage, 150 mm of distance and 3 mL/h of injection rate. The electrospun fibers were subsequently calcinated at different temperatures (600, 650, 700, 800 °C) for 5 h in air at a heating rate of 1 °C min^{-1}.

Table 1 Summary of the quantities of the reagents.

	Sample Code	TEOS (ml)	Ethanol (ml)	1 N HNO_3 (ml)	$Ca(NO_3)_2 \cdot 4H_2O$ (g)	$AgNO_3$ (g)
$70SiO_2$-30CaO	70S30C	3.6	1.85	0.85	1.60	-
$70SiO_2$-28CaO-$2Ag_2O$	70S28C2A	3.6	1.85	0.85	1.49	0.15

2.2. Characterization of cotton-wool-like structured BGs fibers

The morphology of the prepared samples was observed by field emission gun scanning electron microscopy (FEG-SEM) (JSM-6301F, JEOL) with an accelerating voltage of 5 kV after coating the samples with amorphous osmium coater (Neoc, Meiwafosis Co. Ltd.). The fiber diameter was measured using ImageJ software on SEM images, using at least 20 objects for reliable statistics.

Attenuate total reflection-FTIR (ATR-FTIR) (FTIR-4000, JASCO), using a ZnSe crystal, was performed on the fibers. An air background was measured before measuring any samples. Spectra were recorded from 600 to 4000 cm^{-1} with a resolution of 4.0 cm^{-1} and an average of 100 scans. Fiber samples were ground to a fine powder for X-ray diffraction (XRD) (X'Pert X-ray Diffractometer, Philips: CuKα, 50 kV, 40 mA) analysis.

Fibers were imaged using bright field transmission electron microscopy (TEM) (JEM-2100F, JEOL) with an operating voltage of 200 kV. Samples were embedded in epoxy resin, then sectioned using ultramicrotome (EM UC7, Leica). Samples thinner than 100 nm were collected on a TEM grid for imaging.

Nitrogen sorption was performed on a Belsorp-mini II (MicrotracBEL). BG fibers ground to fine powder were loaded into a 1.8 cm^3-sized tube and degassed at 150 °C for 2 h to remove physisorbed gases and water vapor. Twenty adsorption and twenty desorption points were measured. The surface area was calculated from the Brunauer Emmett Teller (BET) method [57] and pore size distributions determined by applying the Barrett Joyner Halenda (BJH) method [58] to the desorption branch of the isotherm [59].

2.3. Dissolution study

A quantity of 2.5 ± 0.05 mg of BG fibers were placed in a 15 mL polypropylene container. To this 5 mL DMEM medium (Gibco) containing 10% fetal bovine serum (FBS) (Gibco) and 1 % penicillin/streptomycin (p/s) (Gibco) was added to start the dissolution test. After sealing the container, the immersed samples were kept in an incubator at 37 °C for 4 – 72 h, under no agitation. At the end of each time period, the media was transferred to a syringe and filtered using a 0.2 μm surfactant-free cellulose

acetate filter (Minisart). The pH of the filtered media was measured using a calibrated pH Electrode 9680 (HORIBA). The ion concentration of the collected media was determined using inductively coupled plasma-atomic emission spectroscopy (ICP-AES, ICPS-7510, Shimadzu). All samples were run in triplicate for statistical analysis and a DMEM alone was incubated under the same conditions and used as a control.

2.4. Antibacterial test

The antibacterial ability of the 70S30C and 70S28C2A fibers with different calcination temperatures were examined using a shake method (Society of Industrial Technology for Antimicrobial Articles) on two different microorganisms: *E. coli* (strain NBRC3972) and *S. aureus* (strain NBRC12732). The medium used was nutrient broth (NB) medium, which was prepared by dissolving 18 g of nutrient broth 'Eiken' (E-MC35, Eiken Chemical Co.) in 1 L of distilled water, followed by autoclaving sterilization at 121 °C for 20 min. The fibers were dry-sterilized at 180 °C for 90 min and then placed in NB medium at a concentration of 0.2 mg/mL. An initial cell concentration of 4 – 5 x 10^4 CFU/mL for *E. coli* was subsequently incubated with the prepared NB medium for 24 h at 37 °C in an orbital-shaking incubator (150 rpm). After the incubation for 24 h, the media with serial dilutions in the range of 10^{-1} to 10^{-10} were prepared. One hundred μL of each dilution was plated onto the agar plate (n = 3). Agar plates were prepared from a standard agar medium, which was prepared by dissolving yeast extract B2 (2.5g, Oriental Yeast Co.), Tryptone (5.0 g, Becton, Dickinson and Co.), D(+)-glucose (1.0 g, Wako Pure Chemical Industries, Ltd.), and Agar (15 g, Wako Pure Chemical Industries, Ltd.) in 1 L of distilled water, followed by autoclaving sterilization at 121 °C for 20 min and poured into plastic petri dish. Fiber-free media cultured under the same conditions was used as control. The numbers of colonies after overnight cultivation were counted [60]. The statistical significance between the Ag-doped samples and between Control and the Ag-doped sample was determined by the Tukey test and Dunnett test, respectively ($p < 0.05$).

2.5. Cell culture test

Mouse fibroblast-like cell line (NIH 3T3) was seeded at a density of 5 x 10^4 cells/mL in 96-well plates with DMEM media supplemented with 10% FBS and 1% p/s. After culturing the cells for 3 h in a humidified incubator with 5 % CO_2, the media was removed and 100 μL of the extracts of each glass fiber sample were added in the 96-well plate. The extracts were prepared by immersing 3.0 mg of glass fibers in 15 mL of the cell culture medium (0.2 mg/mL) and then keeping for 24 h in a biological incubator (37 °C, 120 rpm), followed by filtration with the 0.2 μm filter. The media in each well was changed every other day. The number of the cells in the 96-well plates was counted by using Cell Counting Kit-8 (Dojindo), following the kit's instruction. Briefly, 10 μL of the reaction solution was added in each well and left for 2 h in the CO_2 incubator. A quantity of 80 μL of the solution in each well was moved to another well plate and then the number of the cells in each well was estimated by measuring the absorbance at 450 nm with a multimode plate reader (EnSpire, PerkinElmer) (n = 4). The statistical significance was determined by the Dunnett test ($p < 0.05$).

3. Results and Discussion

3.1. Fiber morphology

A uniform fibrous morphology was observed for the 70S30C and 70S28C2A electrospun materials before and after calcination at different temperatures (Figure 1). The fibers were uniform in size and appeared smooth, forming randomly entangled

architecture in all samples. These results suggested the incorporation of silver did not have any effect on the fibers morphology. The diameter of fibers decreased after calcination, from 329 ± 32 nm to 199 ± 20 nm for 70S30C and from 363 ± 31 nm to 166 ± 20 nm for 70S28C2A, which was due to the removal of solvent and polymer binder within the electrospun fibers at up to 600 °C and then due to densification and increase in silica network connectivity from 600 – 800 °C. All the samples had a cotton-wool-like structure (Figure S1) and there were no noticeable differences in macro-scale appearance between samples with various compositions and calcination temperatures.

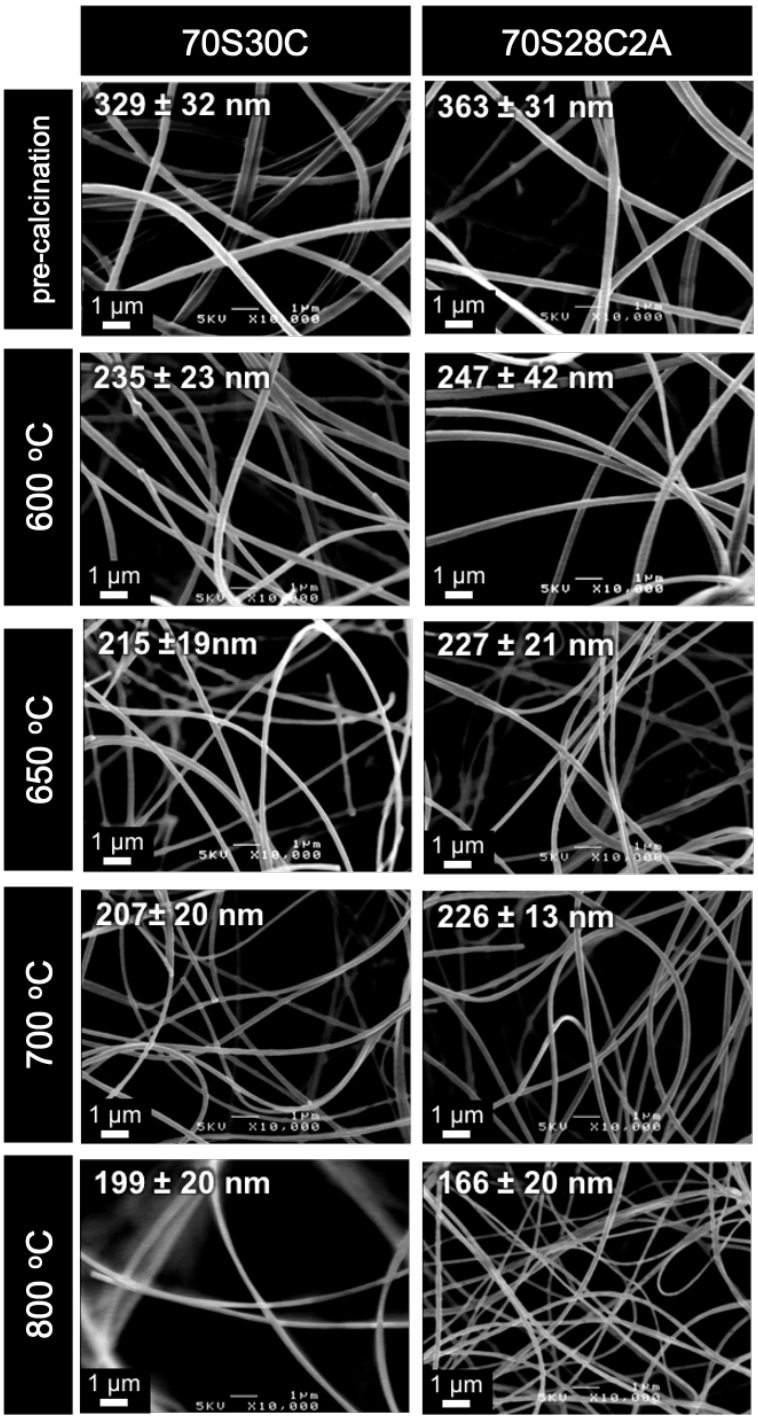

Fig. 1 SEM images of the 70S30C and 70S28C2A samples with different calcination temperatures (The mean ± standard deviation of fiber diameters is shown in each image).

3.2. Chemical structure

Pre-calcination, FTIR spectra of both 70S30C and 70S30C2A showed characteristic bands of sol-gel glasses with two vibration modes of Si-O group (Figure 2a,b). Besides the bands attributed to Si-O-Si and Si-OH, the two bands between wavenumbers 1300-1500 cm^{-1} assigned to N-O from nitrates and a small band at 1640 cm^{-1} assigned to O-H groups of water were observed. This indicates that there were some residual nitrates and solvents trapped in the samples before calcination. This was also confirmed by TG-DTA curves (Fig. S4), which shows weight loss and endothermic peak around 100 °C corresponding to the evaporation of water and exothermic peaks around 400 °C corresponding to the decomposition of nitrates.

After calcination above 600 °C, Si-OH stretching vibration bands among all the samples could not be clearly observed due to removal of some -OH. The band also shifted to around 930 cm^{-1}, characteristic of Si-O non-bridging oxygen associated with incorporation of calcium into the silicate network (Si-O-NBO) [61-63]. The disappearance of the band assigned to N-O and O-H groups was also observed, which means the elimination of nitrate, water and/or alcohol in the samples was successful at this calcination temperature.

Compared to the pre-calcined samples, the Si-O-Si asymmetric bond stretching vibration shifted from 1050 cm^{-1} to lower wavenumbers 1030 cm^{-1} in the spectra of the calcined sample from 600 °C and above. This shift could be related to a structural rearrangement in the Si-O-Si environment leading to lower inter-tetrahedral angle values and a strained network [64]. However, from 700 °C for Ag-doped fibers and 800 °C for 70S30C fibers, this band shifted back to higher wavenumbers, around 1069 cm^{-1}. This behavior can be ascribed to the effect of the crystallization occurring within the surrounding matrix [65]. Furthermore, at 800 °C for Ag-doped fibers and 1000 °C for 70S30C fibers, a new band appeared, which might be due to the crystallization of wollastonite (β–$CaSiO_3$) [66]. Those data suggested that the Ag-doped fibers crystallized at lower temperature than 70S30C fibers.

X-ray diffraction was performed on the samples with and without silver, calcined from 600 to 1000 °C (Figure 2c,d). For the Ag-doped fibers, diffraction peaks corresponding to metallic silver were observed at all calcination temperatures with peaks at 2θ values of 38.1° (111), 44.2° (200), and 64.3° (220). However, it is difficult to say from the XRD data that all the silver was converted into metal as it is possible that some of the silver could exist as ions within the silica network in a similar fashion to that of calcium ions [40]. Carta et al. showed that in conventional sol-gel glass (without electrospinning) that Ag metal nanoparticles are present in the glass, but Ag_2O is also incorporated into the silicate network [40]. In this study, the shape of the diffraction peak evolved as the calcination temperature increased, in specific the intensity increased with reduction of the half-width maximum. This suggests that the size of silver nanoparticles increased with increasing calcination temperature. The mean silver particle sizes were estimated by analyzing the broadening of the (111) reflection using Scherrer's equation,

$$d = \frac{0.9\lambda}{\beta \cos\theta} \qquad (1)$$

where λ is the wavelength of X-ray source (CuKα = 1.54056 Å), and β is the full-width at half-maximum (FWHM) of the X-ray diffraction peak at the diffraction angle θ. Table 2 shows the mean diameter of Ag particles increasing with increasing calcination temperature.

As well as the coarsening of silver other crystalline phases were observed in the XRD data of samples calcined at 1000 °C for 70S30C fibers and 800 °C for Ag-doped fibers. These were identified to be wollastonite, β-$CaSiO_3$, corroborating the observation made by FTIR. It is clear that a larger amount of wollastonite was formed in Ag-doped 70S30C fibers as compared to 70S30C fibers at 800 °C, which also agreed with the FTIR data. Silver is known and has been used in melt-derived glass to promote crystallization by acting as a crystal seed [67]. Thus, the *in situ* formation of metallic silver nanoparticles in the sol-gel glass fibers may have acted as a nucleating agent in a similar fashion to melt-derived glasses.

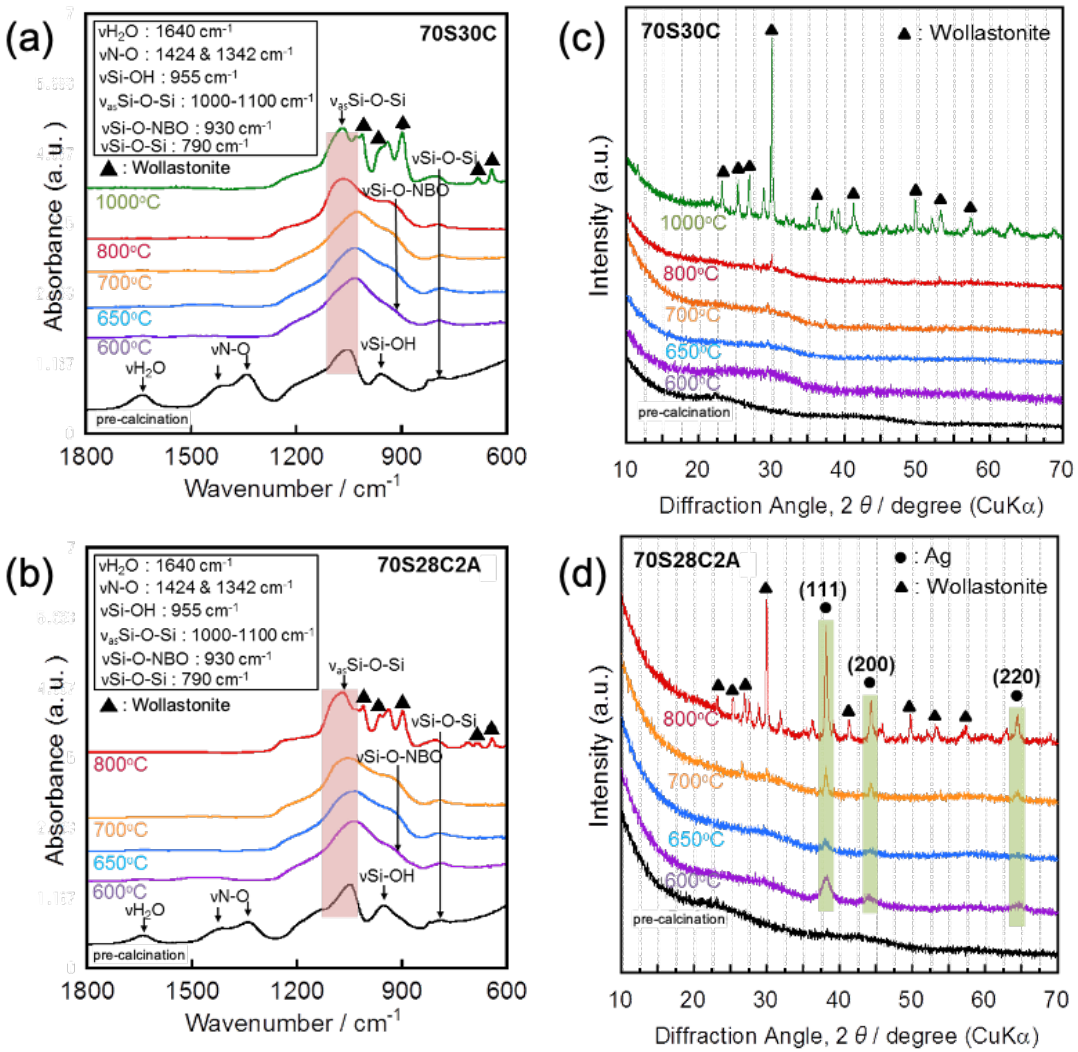

Fig. 2 FTIR spectra (a, b) and XRD (c, d) of the 70S30C (a, c) and 70S28C2A (c, d) samples with different calcination temperatures.

In order to confirm the formation of silver nanoparticles and their distribution within the glass fibers, TEM was performed (Figure 3). Comparing the results of the two samples, it is clear that silver nanoparticles formed in the Ag-doped fibers only after calcination. The size of the silver nanoparticles measured from TEM images increased with increasing calcination temperature (Table 2), from 3 nm following calcination at 600°C to 13 nm after calcination at 700°C and ~26 nm after calcination at 800°C, which agrees with the observations from XRD. It is also clear to observe the migration and growth of silver particles on the TEM images. These are probably driven largely by the

instability of silver atoms due to their high surface free energy. The silver atoms in the glasses might have the ability to move through easily in the silica network with the increased temperature, whereas their moving is normally difficult at room temperature [68]. Their aggregation would produce thermodynamically stable particles with bigger sizes [69].

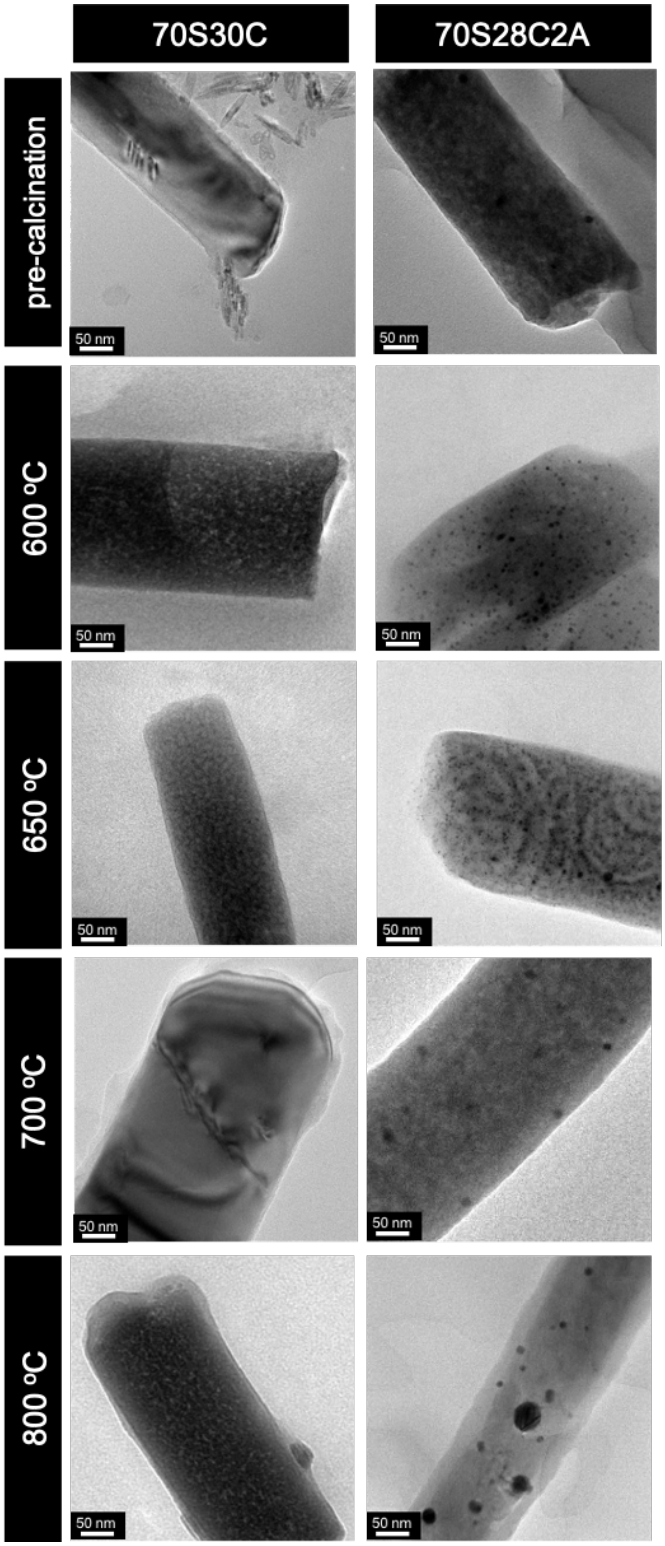

Fig. 3 TEM images of the 70S30C and 70S28C2A samples with different calcination temperature. Scale bar; 50 nm.

Table 2 Silver mean diameter in 70S28C2A samples from Scherrer equation and TEM images at different calcination temperatures.

Temperature (°C)	Mean diameter (nm)	
	Scherrer equation	TEM image
600	9.37	3.68 ± 1.17
650	13.4	3.96 ± 1.35
700	26.9	12.50 ± 1.29
800	30.7	25.98 ± 12.29

3.3. Surface and textural properties

The 70S30C samples before calcination were not porous and so the absorption of nitrogen was mainly monolayer formation followed by saturation on the surface of the fibers leading to a type IV isotherm (Figure S2). The samples calcined at 600 °C, 650 °C, and 700 °C exhibited an increase of specific surface area (SSA) (Table 3). This finding was reported by Lin *et al*. [62], who hypothesized this mechanism for Ca^{2+} incorporation to disrupt the silica network, which is the calcium nitrate covered the nano-texture of silica before calcination. Then, after the nitrate was decomposed, the calcium incorporated into the network of the silica, which increased the surface area. After sintering at 800 °C, the SSA of the samples decreased due to further crosslinking of the SiO_2 network under viscous flow of the glass during sintering. As sintering temperature increased to 800 °C, the pore size was no longer measurable by the BJH method, due to low adsorption of N_2, i.e. there were no pores present or they were smaller than 2 nm.

Table 3 Summary of the values obtained from BET and BJH algorithms of (a) 70S30C and (b) 70S28C2A samples with different calcination temperatures.

(a) 70S30C

Calcination Temperature	Specific Surface area (m^2/g)	C_{BET}	Pore size (nm)	Pore volume (cm^3/g)
Pre-calcination	5.35	56.9	--	--
600 °C	11.0	44.4	51.5	0.0410
650 °C	20.6	130	3.75	0.0461
700 °C	35.6	130	3.75	0.0631
800 °C	12.9	92.6	--	--

(b) 70S28C2A

Calcination Temperature	Specific Surface area (m^2/g)	C_{BET}	Pore (nm)	Pore volume (cm^3/g)
Pre-calcination	12.6	48.3	--	--
600 ºC	25.6	103	6.21	0.0638
650 ºC	18.6	134	5.46	0.0443
700 ºC	17.7	91.6	3.75	0.0407
800 ºC	10.3	70.3	--	--

3.4. Degradation of the BG fibers

Degradation of the prepared samples was evaluated by immersion in the cell culture medium, DMEM, over 3 days. The silica species and calcium ion release profiles (Figure 4a, b, d, e) showed an increase in the concentration with immersion time for all the compositions and calcination temperatures studied. However, differences in their trend were observed. Fibers calcined below 800 °C for 70S30C and below 700 °C for 70S28C2A showed similar trends with a plateau at 60 and 170 mg/L for silicon and calcium, respectively. The 70S28C2A fibers calcined at 700 and 800 °C and the 70S30C fibers calcined at 800 °C showed a slower release rate than the other samples. For those three samples, crystallization occurred and glass-ceramics were formed. The crystallization may have inhibited the silica and calcium release from the glass fibers, especially in the early stages [70]. This could be due to increased network connectivity of the amorphous network.

The amount of calcium released from 70S30C calcined below 700 °C showed a burst release (from 111.1 to 166.3 mg/L) within the first 8 h, while after calcination at 800 °C, the amount of calcium released increased to just 126.5 mg/L and seemed to exhibit a sustained release profile (Figure 4b). This is due to the difference of SSA of the sample (35.6 m^2/g for 700 °C; 12.9 m^2/g for 800 °C), which was caused by the densification of the glass and the crystallization of wollastonite (Figure 2c, d). This suggests that the mesoporous structure could increase Ca^{2+} exchange from the glass fibers with protons from the medium. Concentration of phosphorus in media containing the samples (Figure 4c, f) was in line with that of fiber-free DMEM, which suggests phosphate was not deposited on the glass fibers.

Silver release at 24 h was high for fibers calcined at 650 °C (17 mg/L), whilst fibers calcined at 800 °C had the slowest release (2.4 ml/L) (Figure 4g). Fibers calcined at 700 °C showed a sustained release behavior. From 48 h immersion onwards the release behavior was similar from fibers calcined at 600, 650, and 700 °C. At 72 h, the release amount of silver was around 20 mg/L, while the theoretical value of the concentration in the fibers is 34.5 mg/L, this indicates that <60 at% silver was released by 72 h immersion in the medium. The results indicate that the silver release from the glass fibers could be finely tuned via calcination temperature.

Hydroxyl carbonate apatite (HCA) is formed on surfaces of some bioactive materials after implantation in body. However, our glass fibers are expected to have no ability of such HCA formation from the results of degradation tests; there was no change in the amount of phosphate during the immersion in DMEM (Figure 4c,f). In our previous study, we have observed no HCA formation on the 70S30C glass fibers after immersion

in DMEM for 7 days by XRD[21]. Thus, the glass fibers exhibit the ability of providing therapeutic ions for enhancing tissue regeneration without mineralization.

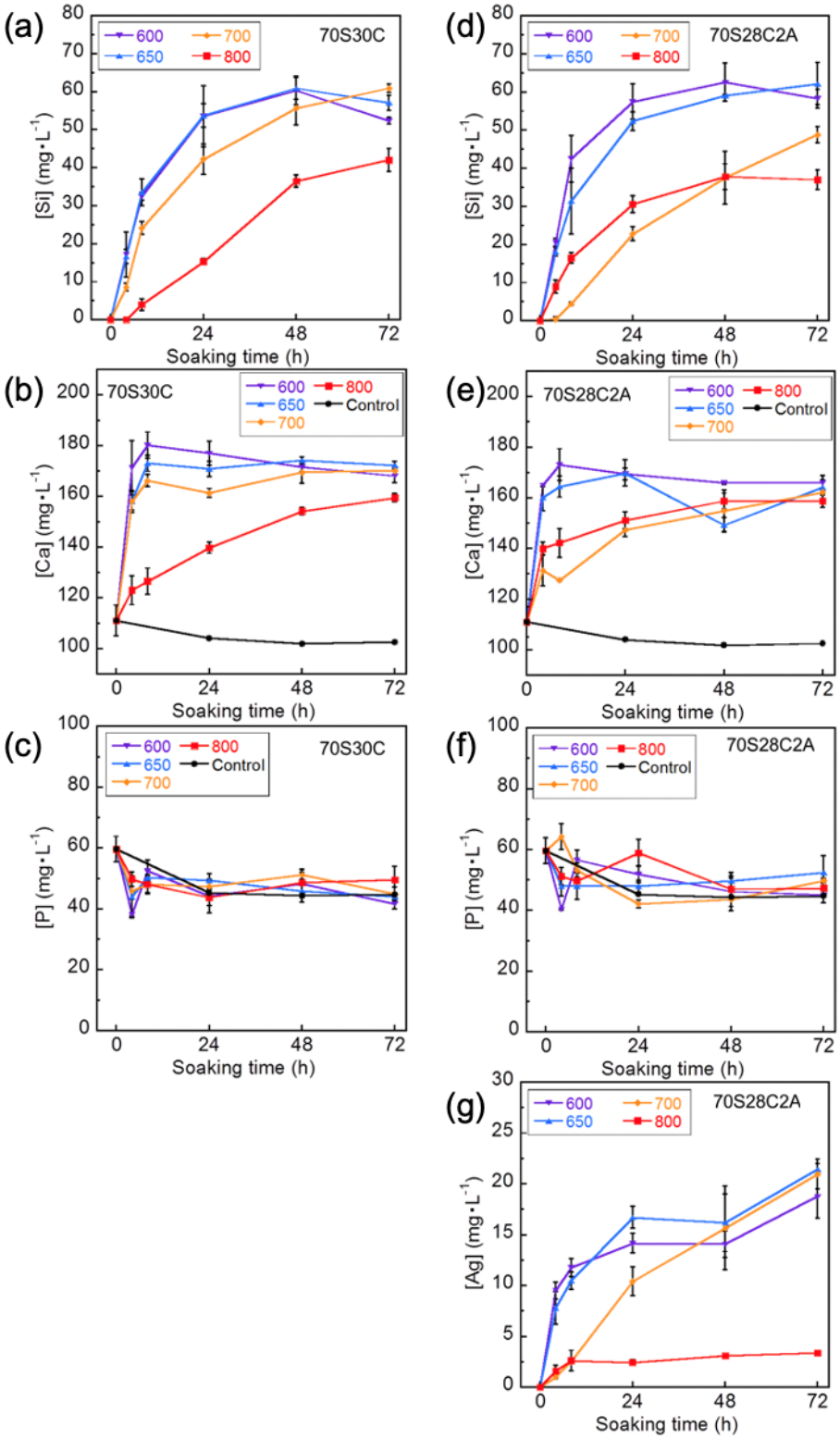

Fig. 4 Elemental concentrations in DMEM after soaking the 70S30C (a-c) and 70S28C2A (d-g) samples with different calcination temperature.

3.5. Antibacterial ability

The bacteriostatic effects of Ag-doped fibers calcined at different temperature on the viability of *E. coli* were investigated. The dependence of colony forming unit (CFU) on the calcination temperatures of 70S30C and 70S28C2A fibers is shown in Figure 5. Sample concentration (weight% in media) is one of the key factors that influence the outcome of antibacterial testes. Therefore, the optimal sample concentration to test the effect of different calcination temperatures on the bacteria was first determined by assessing the antibacterial properties of fibers calcined at 650°C and different concentrations in media (Figure S5a and Table S2 of minimum inhibitory concentration (MIC)). The inhibition of bacterial growth was clearly observed for the samples containing Ag, 70S29C1A (1Ag) and 70S28C2A (2Ag), when the sample concentration was > 0.2 mg/mL, whereas the 70S30C (0Ag) exhibited the same level as that of the control at all sample concentrations studied. In addition, the level of the inhibition depends on the doping level of Ag in the fibers; the bacterial growth was lower for the 70S28C2A than 70S29C1A (Figure S5b). Thus, the antibacterial property of the fibers could be controlled by changing the amount of Ag doping and/or quantity of the fibers used in the construct. These phenomena were observed for both types of bacteria.

A concentration of 0.2 mg/mL fiber in media was used to test the effect of different calcination temperatures on the bacteria (Figure 5). Various concentrations of the different ions in NB medium could be obtained after incubating fibers calcined at different temperatures (Table 4). After 24 h cultivation, no significant differences in the number of *E. coli* between the Ag-free 70S30C samples and the control were observed, while 70S28C2A fibers showed significantly different antibacterial activity ($p < 0.05$) depending on the calcination temperature. The number of CFUs was found to be lower at low calcination temperature, even though there was no significant difference in the concentration of silver in NB medium after soaking the samples calcined at 600, 650 and 700 °C (Table 4, between 6 and 7.5 mg/L). The amount of silver released from the sample calcinated at 800°C in NB medium reduced to ~1 mg/L in comparison with that of the other samples.

A correlation between the size of the silver nanoparticles in the fibers and antibacterial activity was found where increase in size leads to reduced antibacterial activity. As the size of silver nanoparticles in the 70S28C2A fibers increased from ~4 nm at 650 °C to 12.5 nm at 700 °C (Table 2), not a significantly different amount of silver was released from the fibers into the media however a steady state release was observed for the 700 °C (Figure 4). Once the fibers were calcined to 800 °C significantly lower amount of silver was released into the media (1 mg/L). The nanoparticle size further increased to 26 nm at this calcination temperature (Table 2). The increase in size of the nanoparticles seems to be one of the main factors determining the release rate of Ag from the fibers as specific surface area of the calcined fibers were similar (Table 3). Sotiriou *et al*. reported that, Ag nanoparticle in the size range of 4 to 10 nm, the smaller sized particles exhibited a stronger antimicrobial ability even though their concentration was small, 1 mg/L [55]. This was because the smaller nanoparticles had a larger SSA and released larger amount of silver ions. Thus, the amount of silver ions released from the nanoparticles play a strong antimicrobial role. In the present work, silver nanoparticles with < 12.5 nm were incorporated in the 70S28C2A calcined at 600, 650 and 700°C. It is possible that during incubation the silver nanoparticles could react with the NB medium following absorption into the glass mesopores via capillary forces. The smaller nanoparticles have higher surface area and are distributed over larger area in the glass fibers hence are much more effective at releasing the silver

ions. On the other hand, Sotiriou *et al*. also reported that not only silver ions but nanoparticles themselves play an antimicrobial role in the case of larger silver nanoparticles (> 10 nm) [55]. A stronger antimicrobial activity was observed when both silver ions and nanoparticles were provided to bacteria, in comparison with when providing only silver ions. However, such larger nanoparticles, of course, released smaller amount of silver ions because of their smaller SSA. Therefore, these phenomena were observed only when a large amount of the nanoparticles was provided to bacteria (> 20 mg/L). Fabrega *et al*. reported that bacterial contact with silver nanoparticles (>50 nm in size) plays a predominant role in antimicrobial activity [71]. From the TEM observation (Figure 3), few nanoparticles were present at the area near the fiber surface. This might contribute to the minimal amount of released silver nanoparticles and subsequent poor antimicrobial efficacy of the 70S28C2A calcined at 800°C.

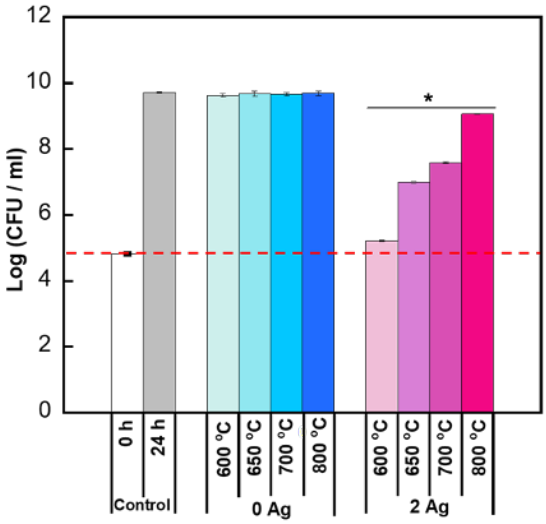

Fig. 5 Number (log CFU/mL) of *E.coli* after 24 h cultivation with the 70S30C (0Ag) and 70S28C2A (2Ag) samples with different calcination temperatures. (dotted line; the level of Control sample before cultivation) (* p<0.05 vs Control@24 h).

Table 4 Elemental concentration in Nutrient broth (NB) medium after soaking the 70S30C (0Ag) or 70S28C2A (2Ag) fibers with different calcination temperature for 24 h.

Sample (glass- calcination temperature)	[Si] (mg/L)	[Ca] (mg/L)	[Ag] (mg/L)
Control	0	13.6±0.5	0
0Ag-600	47.3±2.9	66.8±3.7	0
0Ag-650	48.5±0.5	72.0±2.4	0
0Ag-700	26.4±2.2	61.3±5.8	0
0Ag-800	8.0±0.6	48.7±3.2	0
2Ag-600	33.8±0.6	57.8±1.4	6.7±0.3
2Ag-650	31.0±3.4	60.0±3.9	7.5±0.8

2Ag-700	22.0±1.6	61.7±4.0	6.0±0.5
2Ag-800	19.1±0.4	58.7±1.0	1.2±0.1

3.6. Cell compatibility

Cytotoxicity tests for the 70S30C and 70S28C2A samples using fibroblasts were evaluated. The cytotoxicity of both the samples showed the dependence on the calcination temperature. Media from the fibers calcined at 600°C with both the compositions caused some toxicity, but the number of viable cells increased with increasing sample calcination temperature (Figure 6). This is due to the burst release of ions in the first 24 h from the samples calcined at lower temperature (Figure 4). Media from the 70S28C2A samples calcined at 650°C and 700°C showed reduced toxicity, while the 70S28C2A sample calcined at 800 °C had significantly higher number of viable cells than the control both at 24 and 72 h. This sample releases smaller amounts of silicate species and calcium ions. In addition, the release amount of silver ions was also smaller than the others, which affected cell proliferation. The size of silver nanoparticles is also expected to relate to cytotoxicity; the larger nanoparticles released from the sample calcined at 800 °C may possess a lower cytotoxicity. All the samples except those calcined at 600 °C exhibited cell proliferation over 72 h and the proliferation rate most likely depends on the calcination temperatures for the glass fibers.

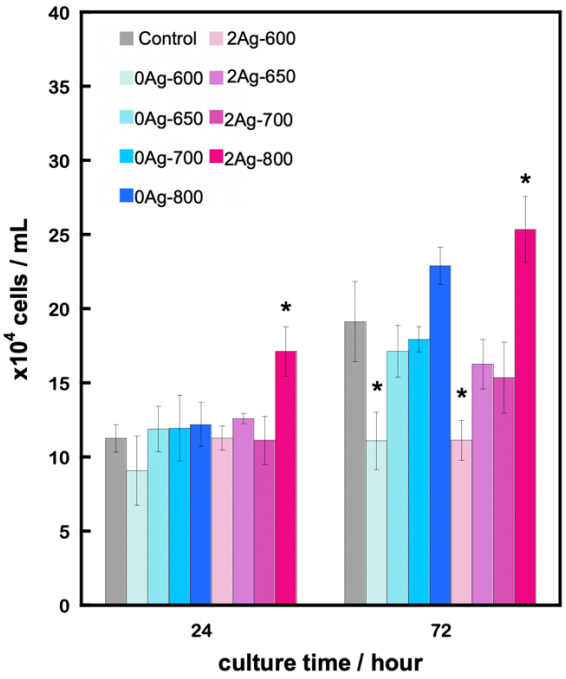

Fig. 6 Number of live fibroblasts after cultivation with extract of the 70S30C (0Ag) and 70S28C2A (2Ag) samples with different calcination temperatures. (* p<0.01 vs Control).

4. Conclusion

Ag-doped bioactive glasses with 3D cotton-wool-like structure were prepared combining sol-gel processing and electrospinning techniques. The calcination temperatures for the samples after electrospinning was found to influence the state of

Ag in the glass fibers, with nanoparticles forming and coarsening, as the calcination temperature increased, which strongly correlated to their antibacterial property and cell compatibility. Silver was observed to become metallic nanoparticles on calcination, which increased in size as calcination temperature increased, decreasing antimicrobial properties of the fibers. As the size of silver nanoparticles in the fibers increased from 12.5 nm to 26 nm as calcination temperature increased, which resulted in the amount of silver in the media decreasing to 1 mg/L, reducing antimicrobial efficacy. The reduction in antimicrobial activity was attributed to the size of the nanoparticles as there was no reduction in the release rate of calcium cations. These results suggests that not only the amount of silver but also the calcination temperature plays a significant role on influencing properties of Ag-doped sol-gel glasses. In addition, Ag nanoparticles particularly grew in the area close to the center of the glass fiber after the calcination treatment in comparison with those close to surfaces, which is also one of the factors influencing properties of the glasses. These unique behaviors of Ag doped in the electrospun glass fibers were revealed in the first time in the present study. Since it is possible to control properties of the Ag-doped 3D glass fibers developed in the present study, they could have a significant impact in the treatment of chronic wounds.

Funding
This work was supported by the JSPS KAKENHI Grant Number 18K12075, Nippon Sheet Glass Foundation for Materials Science and Engineering and the Hibi Science Foundation.

Conflict of interest
The authors declare that they have no conflict of interest.

References

[1] A.D. Metcalfe, M.W.J. Ferguson, Biomaterials, 28 (2007) 5100-5113. https://doi.org/10.1016/j.biomaterials.2007.07.031.
[2] G.C. Gurtner, S. Werner, Y. Barrandon, M.T. Longaker, Nature, 453 (2008) 314-321. https://doi.org/10.1038/nature07039.
[3] M.J. Carter, K. Tingley-Kelley, R.A. Warriner, III, Journal of the American Academy of Dermatology, 63 (2010) 668-679. https://doi.org/10.1016/j.jaad.2009.09.007.
[4] R.G. Frykberg, J. Banks, Advances in Wound Care, 4 (2015) 560-582. https://doi.org/10.1089/wound.2015.0635.
[5] P.G. Bowler, B.I. Duerden, D.G. Armstrong, Clinical Microbiology Reviews, 14 (2001) 244. https://doi.org/10.1128/CMR.14.2.244-269.2001.
[6] S. Kargozar, S. Hamzehlou, F. Baino, Mater. Sci. Eng. C, 97 (2019) 1009-1020. https://doi.org/10.1016/j.msec.2019.01.028.
[7] S. Kargozar, M. Mozafari, S. Hamzehlou, F. Baino, Frontiers in Bioengineering and Biotechnology, 7 (2019). https://doi.org/10.3389/fbioe.2019.00062.
[8] S.G. Kumbar, R. James, S.P. Nukavarapu, C.T. Laurencin, Biomed. Mater., 3 (2008) 034002. https://doi.org/10.1088/1748-6041/3/3/034002.
[9] S.G. Priya, H. Jungvid, A. Kumar, Tissue Engineering Part B: Reviews, 14 (2008) 105-118. https://doi.org/10.1089/teb.2007.0318.
[10] N. Ferrara, Am J Physiol Cell Physiol, 280 (2001) C1358-1366. https://doi.org/10.1152/ajpcell.2001.280.6.C1358.

[11] M. Simons, J.A. Ware, Nature Reviews Drug Discovery, 2 (2003) 863-872. https://doi.org/10.1038/nrd1226.
[12] A. Hoppe, N.S. Güldal, A.R. Boccaccini, Biomaterials, 32 (2011) 2757-2774. https://doi.org/10.1016/j.biomaterials.2011.01.004.
[13] C. Lin, C. Mao, J. Zhang, Y. Li, X. Chen, Biomed. Mater., 7 (2012) 045017. https://doi.org/10.1088/1748-6041/7/4/045017.
[14] R.M. Day, A.R. Boccaccini, S. Shurey, J.A. Roether, A. Forbes, L.L. Hench, S.M. Gabe, Biomaterials, 25 (2004) 5857-5866. https://doi.org/10.1016/j.biomaterials.2004.01.043.
[15] A. Leu, J.K. Leach, Pharm Res, 25 (2008) 1222-1229. https://doi.org/10.1007/s11095-007-9508-9.
[16] A.A. Gorustovich, J.A. Roether, A.R. Boccaccini, Tissue Eng Part B Rev, 16 (2010) 199-207. https://doi.org/10.1089/ten.TEB.2009.0416.
[17] H. Li, K. Xue, N. Kong, K. Liu, J. Chang, Biomaterials, 35 (2014) 3803-3818. https://doi.org/10.1016/j.biomaterials.2014.01.039.
[18] K. Dashnyam, A. El-Fiqi, J.O. Buitrago, R.A. Perez, J.C. Knowles, H.W. Kim, J Tissue Eng, 8 (2017) 2041731417707339. https://doi.org/10.1177/2041731417707339.
[19] A. Leu, S.M. Stieger, P. Dayton, K.W. Ferrara, J.K. Leach, Tissue Eng Part A, 15 (2009) 877-885. https://doi.org/10.1089/ten.tea.2008.0018.
[20] R. Li, A.E. Clark, L.L. Hench, J. Appl. Biomater., 2 (1991) 231-239. https://doi.org/10.1002/jab.770020403.
[21] E. Norris, C. Ramos-Rivera, G. Poologasundarampillai, J.P. Clark, Q. Ju, A. Obata, J.V. Hanna, T. Kasuga, C.A. Mitchell, G. Jell, J.R. Jones, Biomed. Mater., 15 (2020) 015014. https://doi.org/10.1088/1748-605x/ab591d.
[22] A.R. Shahverdi, A. Fakhimi, H.R. Shahverdi, S. Minaian, Nanomedicine: Nanotechnology, Biology and Medicine, 3 (2007) 168-171. https://doi.org/10.1016/j.nano.2007.02.001.
[23] N. Pajares-Chamorro, Y. Wagley, C.V. Maduka, D.W. Youngstrom, A. Yeger, S.F. Badylak, N.D. Hammer, K. Hankenson, X. Chatzistavrou, Mater. Sci. Eng. C, 120 (2021) 111693. https://doi.org/10.1016/j.msec.2020.111693.
[24] M. Bellantone, N.J. Coleman, L.L. Hench, J. Biomed. Mater. Res., 51 (2000) 484-490. https://doi.org/10.1002/1097-4636(20000905)51:3<484::AID-JBM24>3.0.CO;2-4.
[25] N. Azizabadi, P.A. Azar, M.S. Tehrani, P. Derakhshi, J. Non-Cryst. Solids., 556 (2021) 120568. https://doi.org/10.1016/j.jnoncrysol.2020.120568.
[26] C.Y.K. Lung, M.M. Abdalla, C.H. Chu, I. Yin, S.-R. Got, J.P. Matinlinna, Materials, 14 (2021) 961. https://doi.org/10.3390/ma14040961.
[27] M. Zohourfazeli, M.H. Mahdi Tajer, A. Moghanian, Ceram. Int., 47 (2021) 2499-2507. https://doi.org/10.1016/j.ceramint.2020.09.093.
[28] A. Feraru, Z.R. Tóth, K. Magyari, Z. Pap, M. Todea, M. Mureşan-Pop, D.C. Vodnar, E. Licarete, K. Hernadi, L. Baia, J. Non-Cryst. Solids., 547 (2020) 120293. https://doi.org/10.1016/j.jnoncrysol.2020.120293.
[29] L.D. Soule, N. Pajares Chomorro, K. Chuong, N. Mellott, N. Hammer, K.D. Hankenson, X. Chatzistavrou, ACS Biomaterials Science & Engineering, 6 (2020) 5549-5562. https://doi.org/10.1021/acsbiomaterials.0c01140.
[30] M.S.N. Shahrbabak, F. Sharifianjazi, D. Rahban, A. Salimi, Silicon, 11 (2019) 2741-2751. https://doi.org/10.1007/s12633-018-0063-2.

[31] A.C. Vale, P.R. Pereira, A.M. Barbosa, E. Torrado, N.M. Alves, Mater. Sci. Eng. C, 94 (2019) 161-168. https://doi.org/10.1016/j.msec.2018.09.027.
[32] A.A. El-Rashidy, G. Waly, A. Gad, J.A. Roether, J. Hum, Y. Yang, R. Detsch, A.A. Hashem, I. Sami, W.H. Goldmann, A.R. Boccaccini, Biomed. Mater., 13 (2018) 065006. https://doi.org/10.1088/1748-605x/aad8cf.
[33] B. Aksakal, M. Demirel, Proceedings of the Institution of Mechanical Engineers, Part H: Journal of Engineering in Medicine, 232 (2018) 1039-1047. https://doi.org/10.1177/0954411918797968.
[34] A.C. Vale, A.L. Carvalho, A.M. Barbosa, E. Torrado, J.F. Mano, N.M. Alves, Adv. Eng. Mater., 20 (2018) 1700855. https://doi.org/10.1002/adem.201700855.
[35] F.E. Ciraldo, L. Liverani, L. Gritsch, W.H. Goldmann, A.R. Boccaccini, Materials, 11 (2018) 692. https://doi.org/10.3390/ma11050692.
[36] A.A. El-Rashidy, G. Waly, A. Gad, A.A. Hashem, P. Balasubramanian, S. Kaya, A.R. Boccaccini, I. Sami, J. Non-Cryst. Solids., 483 (2018) 26-36. https://doi.org/10.1016/j.jnoncrysol.2017.12.044.
[37] S. Kaya, M. Cresswell, A.R. Boccaccini, Mater. Sci. Eng. C, 83 (2018) 99-107. https://doi.org/10.1016/j.msec.2017.11.003.
[38] E.G. Pires, R.F. Bonan, Í.M. Rocha, I.M.F. Gonçalves, J.R. de Souza, L.H.V. Gonzales, J.V.J. Silva Júnior, D.E.d.C. Perez, P.C.B. Tavares, S.M.d. Silva, R.P. Alves-Balvedi, L.R. Goulart, E.S. de Medeiros, L.R. Castellano, P.R.F. Bonan, Int. J. Appl. Glass Sci., 9 (2018) 52-61. https://doi.org/10.1111/ijag.12285.
[39] F. Sharifianjazi, N. Parvin, M. Tahriri, Ceram. Int., 43 (2017) 15214-15220. https://doi.org/10.1016/j.ceramint.2017.08.056.
[40] D. Carta, J.R. Jones, S. Lin, G. Poologasundarampillai, R.J. Newport, D.M. Pickup, Int. J. Appl. Glass Sci., 8 (2017) 364-371. https://doi.org/10.1111/ijag.12318.
[41] F. Sharifianjazi, N. Parvin, M. Tahriri, J. Non-Cryst. Solids., 476 (2017) 108-113. https://doi.org/10.1016/j.jnoncrysol.2017.09.035.
[42] T. Fu, Z. Alajmi, Y. Shen, L. Wang, S. Yang, M. Zhang, Int. J. Appl. Ceram. Technol., 14 (2017) 1117-1124. https://doi.org/10.1111/ijac.12713.
[43] S. Naseri, W.C. Lepry, S.N. Nazhat, J. Mater. Chem. B, 5 (2017) 6167-6174. https://doi.org/10.1039/C7TB01221G.
[44] J. Rivadeneira, A. Gorustovich, Journal of Applied Microbiology, 122 (2017) 1424-1437. https://doi.org/10.1111/jam.13393.
[45] Y.-F. Goh, A.Z. Alshemary, M. Akram, M.R. Abdul Kadir, R. Hussain, Int. J. Appl. Glass Sci., 5 (2014) 255-266. https://doi.org/10.1111/ijag.12061.
[46] H. Zhu, C. Hu, F. Zhang, X. Feng, J. Li, T. Liu, J. Chen, J. Zhang, Mater. Sci. Eng. C, 42 (2014) 22-30. https://doi.org/10.1016/j.msec.2014.05.004.
[47] H. Palza, B. Escobar, J. Bejarano, D. Bravo, M. Diaz-Dosque, J. Perez, Mater. Sci. Eng. C, 33 (2013) 3795-3801. https://doi.org/10.1016/j.msec.2013.05.012.
[48] A. Vulpoi, L. Baia, S. Simon, V. Simon, Mater. Sci. Eng. C, 32 (2012) 178-183. https://doi.org/10.1016/j.msec.2011.10.015.
[49] A.M. El-Kady, A.F. Ali, R.A. Rizk, M.M. Ahmed, Ceram. Int., 38 (2012) 177-188. https://doi.org/10.1016/j.ceramint.2011.05.158.
[50] M.G. Raucci, K. Adesanya, L. Di Silvio, M. Catauro, L. Ambrosio, J. Biomed. Mater. Res. Part B, 92B (2010) 102-110. https://doi.org/10.1002/jbm.b.31495.
[51] A. Balamurugan, G. Balossier, D. Laurent-Maquin, S. Pina, A.H.S. Rebelo, J. Faure, J.M.F. Ferreira, Dent. Mater., 24 (2008) 1343-1351. https://doi.org/10.1016/j.dental.2008.02.015.

[52] M. Catauro, M.G. Raucci, F. de Gaetano, A. Marotta, J. Mater. Sci.-Mater. Med., 15 (2004) 831-837. https://doi.org/10.1023/B:JMSM.0000032825.51052.00.
[53] S. Saha, A. Bhattacharjee, S.H. Rahaman, S. Ray, M.K. Marei, H. Jain, J. Chakraborty, Int. J. Appl. Glass Sci., 11 (2020) 320-328. https://doi.org/10.1111/ijag.15029.
[54] X. Qin, R. Cao, J. Zheng, G. Shi, L. Ji, A. Zhu, H. Yao, RSC Adv., 10 (2020) 44835-44840. https://doi.org/10.1039/D0RA08656H.
[55] G.A. Sotiriou, S.E. Pratsinis, Environmental Science & Technology, 44 (2010) 5649-5654. https://doi.org/10.1021/es101072s.
[56] H.W. Kim, H.E. Kim, J.C. Knowles, Adv. Funct. Mater., 16 (2006) 1529-1535. https://doi.org/10.1002/adfm.200500750.
[57] S. Brunauer, L.S. Deming, W.E. Deming, E. Teller, J. Am. Chem. Soc., 62 (1940) 1723-1732. https://doi.org/10.1021/ja01864a025.
[58] E.P. Barrett, L.G. Joyner, P.P. Halenda, J. Am. Chem. Soc., 73 (1951) 373-380. https://doi.org/10.1021/ja01145a126.
[59] K.S.W. Sing, Pure Appl. Chem., 57 (1985) 603-619. https://doi.org/10.1351/pac198557040603.
[60] S. Lee, H. Uehara, A.L.B. Maçon, H. Maeda, A. Obata, K. Ueda, T. Narushima, T. Kasuga, Mater. Trans., 57 (2016) 2072-2076. https://doi.org/10.2320/matertrans.MI201503.
[61] J. Serra, P. González, S. Liste, C. Serra, S. Chiussi, B. León, M. Pérez-Amor, H.O. Ylänen, M. Hupa, J. Non-Cryst. Solids., 332 (2003) 20-27. https://doi.org/10.1016/j.jnoncrysol.2003.09.013.
[62] S. Lin, C. Ionescu, K.J. Pike, M.E. Smith, J.R. Jones, J. Mater. Chem., 19 (2009) 1276-1282. https://doi.org/10.1039/b814292k.
[63] P. Innocenzi, P. Falcaro, D. Grosso, F. Babonneau, The Journal of Physical Chemistry B, 107 (2003) 4711-4717. https://doi.org/10.1021/jp026609z.
[64] A.K. Sandhu, S. Singh, O.P. Pandey, Journal of Physics D: Applied Physics, 41 (2008) 165402. https://doi.org/10.1088/0022-3727/41/16/165402.
[65] T. Van Tran, S. Turrell, M. Eddafi, B. Capoen, M. Bouazaoui, P. Roussel, S. Berneschi, G. Righini, M. Ferrari, S.N.B. Bhaktha, O. Cristini, C. Kinowski, J. Mol. Struct., 976 (2010) 314-319. https://doi.org/10.1016/j.molstruc.2010.04.010.
[66] S. Atalay, H.I. Adiguzel, F. Atalay, Materials Science and Engineering: A, 304-306 (2001) 796-799. https://doi.org/10.1016/S0921-5093(00)01572-0.
[67] P.W. McMillan, J. Non-Cryst. Solids., 52 (1982) 67-76. https://doi.org/10.1016/0022-3093(82)90281-2.
[68] E.D. Martínez, M.G. Bellino, G.J.A.A. Soler-Illia, ACS Appl. Mater. Interfaces, 1 (2009) 746-749. https://doi.org/10.1021/am900018j.
[69] Q. Zhang, D. Wu, S. Qi, Z. Wu, X. Yang, R. Jin, Materials Letters, 61 (2007) 4027-4030. https://doi.org/10.1016/j.matlet.2007.01.011.
[70] C. Durucan, B. Akkopru, J. Biomed. Mater. Res. Part B, 93B (2010) 448-458. https://doi.org/10.1002/jbm.b.31602.
[71] J. Fabrega, S.R. Fawcett, J.C. Renshaw, J.R. Lead, Environmental Science & Technology, 43 (2009) 7285-7290. https://doi.org/10.1021/es803259g.